Desalination and Water Treatment
www.deswater.com

doi: 10.1080/19443994.2016.1138331

57 (2016) 23844–23855
October

Taylor & Francis
Taylor & Francis Group

A novel high efficient Mg–Ce–La adsorbent for fluoride removal: kinetics, thermodynamics and reusability

Liying Wu[a], Gaoke Zhang[b,*], Dandan Tang[a]

[a]*School of Resources and Environmental Engineering, Wuhan University of Technology, 122 Luoshi Road, Wuhan 430070, China, Tel. +86 27 87651816; Fax: +86 27 87887445; email: wuliying19911217@163.com (L. Wu), tangdd0802@126.com (D. Tang)*
[b]*Hubei Key Laboratory of Mineral Resources Processing and Environment and School of Resources and Environmental Engineering, Wuhan University of Technology, 122 Luoshi Road, Wuhan 430070, China, Tel. +86 27 87651816; Fax: +86 27 87887445; email: gkzhang@whut.edu.cn*

Received 5 September 2015; Accepted 30 December 2015

ABSTRACT

A novel Mg–Ce–La adsorbent was prepared by a facile co-precipitation method and was used for fluoride removal. The as-obtained adsorbent has a large specific surface area of 118.6 m^2/g and exhibited high fluoride removal efficiency of 97.5%, which may be attributed to the ion-exchange between the hydroxyl ion and fluoride ion. The fluoride adsorption over the Mg–Ce–La adsorbent could reach its equilibrium in about 40 min and follow the Freundlich model and the pseudo-second-order model. In addition, the Mg–Ce–La adsorbent showed high adsorption performance over a wide pH range from 3.0 to 8.0 for fluoride removal, which would be beneficial for practical application. Finally, the Mg–Ce–La adsorbent still exhibited high fluoride removal rate after four reused cycles.

Keywords: Fluorine; Mg–Ce–La adsorbent; Adsorption

1. Introduction

Fluoride is one of the most abundant elements in the earth. Fluoride contamination is a major problem worldwide, which mainly results from natural reasons and human activities [1]. Fluoride is related to the human health. Excess fluoride in drinking water can cause fluorosis, dental, and skeletal [2,3]. WHO has recommended a guidance value of 1.5 mg/L for fluoride in drinking water, and the permissible concentration of fluoride ions is less than 1.0 mg/L in China [4].

There are many methods for fluoride removal from drinking water, such as reverse osmosis, nanofiltration, electrodialysis, electrocoagulation, Donnan dialysisi, and ion-exchange [5–12]. Although they have already been modernized, these methods are still tedious and time-consuming [13]. Adsorption is a more acceptable defluoridation method and is extensively used because of the simplicity of design, environmental considerations, effectiveness, and convenience as compared to other methods [14,15]. Recently, many adsorbents have been investigated for fluoride removal [16,17], such as activated alumina [18,19], clay [20], geomaterials [21], and quicklime [22]. Among these adsorbents, activated alumina, as the most common adsorbent, is often used to remove excess fluoride ions from water because it is readily available [18,23]. However, its optimal adsorption works at a narrow range of pH and excess alumina may result in extra operation difficulty and secondary pollution problems. The adsorption capacity

*Corresponding author.

of most conventional adsorbents is not very satisfactory [24,25]. Therefore, it is important to develop novel, high adsorption capacity and high-effective fluoride adsorbents.

La(III), Ce(IV), and Zr(IV) oxides have high adsorption capacity for fluoride because of their strong affinity to fluoride [26,27]. Raichur reported that a mixed rare earth metal oxide is very effective for removing fluoride [26]. Mixing rare earth metal elements with cheaper components would keep high fluoride adsorption capacity [28], such as Ce-Fe oxide [29,30]. In addition, the hybrid adsorbents are effective on defluoridation, such as the Fe(III)-Zr(IV) hybrid oxide [28] and Zn-Al layered double hydroxides [31]. Furthermore, some bimetal adsorbents and trimetal oxide adsorbent also present very promising potential for fluoride removal, such as the Mg-Al bimetallic oxides [32] and Fe–Al–Ce trimetal oxide adsorbent [1,25].

In this paper, the novel Mg–Ce–La adsorbent with high adsorption capacity was prepared by a facile precipitation method. The preparation conditions and the adsorption parameters were investigated in detail. Finally, the adsorption mechanism of the Mg–Ce–La adsorbent was proposed, and reuse of the Mg–Ce–La adsorbent was evaluated.

2. Experimental

2.1. Materials and methods

All chemicals used in this paper study were of analytical reagent grade. Standard stock fluoride solution (100 mg/L) was prepared by dissolving 0.2210 g anhydrous sodium fluoride to 1000.00 mL of distilled water at ambient condition. The working solutions of required concentration were prepared by appropriate dilutions of the stock solution.

A series of $Ce(NO_3)_3{\cdot}6H_2O$, $Mg(NO_3)_2{\cdot}6H_2O$, and $La(NO_3)_3{\cdot}nH_2O$ were dissolved in 200 mL of distilled water to form a mixed solution under a temperature of 343 K with magnetic stirrers. The pH of the mixed solution was adjusted to 8.5 by dropwise adding 3-M NaOH solution, and then the solution was stirred for 2 h. The precipitate was then centrifuged and washed with distilled water until the pH of the filtrate was 7.0 ± 0.2. The residual solid was collected, treated at different temperature (343, 353, 473, 573, and 773 K) for 6 h. Finally, it was ground to fine powder.

2.2. Characterization

X-ray diffraction analysis was carried out in a Japan D/MAX-RB powder diffractometer equipping with Cu Kα radiation (40 kV and 50 mA) at a scanning speed of 15°/min from 3° to 70°. The chemical bonds of the surface on Mg–Ce–La adsorbent before and after defluoridation were examined by Fourier transform infrared (FT-IR) spectroscopy at wavenumber from 400 to 4,000 cm^{-1}. N_2 adsorption and desorption experiments were conducted in order to calculate the specific surface area using BET model. The surface bonding analysis of the Mg–Ce–La adsorbent before and after adsorption of fluoride was carried out using X-ray photoelectron spectroscopy (XPS) (VG Multilab 2000, America). The element composition was measured by energy-dispersive X-ray spectroscopy (EDX, JSM-5610LV).

2.3. Fluoride adsorption experiments

About 100 mL of fluoride solution with concentration of 10 mg/L and 1.0 g/L of adsorbent were added into conical flask, and then the flasks were shaken at 180 rpm and kept at 303 K for required time. The effects of the Mg–Ce–La adsorbent dose (0.2–2.0 g/L), initial fluoride pH (3.0–10.0), temperature (293–323 K), and concentration (10–50 mg/L) were investigated by batch adsorption experiments. The effects of coexisting anions such as chloride, nitrate, carbonate, bicarbonate, and sulfate were tested on fluoride adsorption. For examining the adsorption isotherm and kinetic of fluoride on the Mg–Ce–La adsorbent, a series of adsorption experiments were conducted using 1.0 g/L of adsorbent at pH 5.0–6.0.

The adsorption capacity of fluoride and removal rate were calculated using follow equations:

$$q_e = (C_0 - C_e)(V/m) \times 100 \quad (1)$$

$$u = \frac{(C_0 - C_e)}{C_0} \times 100\% \quad (2)$$

In Eqs. (1) and (2), q_e and u are the adsorption capacity (mg/g) and removal ratio (%) separately; C_0 and C_e are initial and equilibrium concentrations of fluoride (mg/L), respectively; V is volume of the aqueous solution (L) and m is the mass (g) of the Mg–Ce–La adsorbent used in the experiment.

2.4. Desorption and cycle experiments

Desorption experiments were carried out in order to examine the desorption capacity of the Mg–Ce–La adsorbent. About 0.1 g of the Mg–Ce–La adsorbent was added into 100 mL of 10 mg/L fluoride solution, and the adsorption process was conducted with shaking speed of 180 rpm and temperature of 303 K for

2 h. Then, the suspension was centrifuged and the used adsorbent was collected. The used adsorbent was suspended in 100 mL of NaOH solution (0.25 M). The reaction was conducted with vigorously shaking for 4 h. Then the precipitate was centrifuged and washed with distilled water until the pH of the filtrate was 7.0 ± 0.2, and then dried at 353 K for 5 h. Finally, the regenerated adsorbent was obtained.

For examining the adsorption potential of the regenerated adsorbent, cycle experiments were conducted at the same initial conditions.

3. Results and discussion

3.1. Optimization of preparation conditions for the Mg–Ce–La adsorbent

3.1.1. Effect of Mg/La/Ce molar ratio

Fig. 1(a) shows the fluoride removal over the as-obtained samples under different molar ratios of Mg (II), La(III), and Ce(III). The fluoride removal rate on the samples with 0.5:4:2, 1:4:2, 1.5:4:2, 1:3:2, 1:5:2, 1:4:1, and 1:4:3 molar ratio of Mg(II), La(III), and Ce(III) was of 90.5, 97.8, 90.2, 62.1, 75.3, 84.5, and 85.7%, respectively. Obviously, the sample with 1:4:2 molar ratio of Mg/Ce/La exhibited the higher fluoride removal property. Thus, the fluoride removal can be affected by the proportion of La(III), Ce(III), and Mg(II).

3.1.2. Effect of treatment temperature

The removal of fluoride by the Mg–Ce–La adsorbent treated under different temperatures is shown in Fig. 1(b). Obviously, the fluoride removal efficiency of the obtained adsorbents increased with increasing treatment temperature from 343 to 353 K, and then decreased with further increasing the temperature from 353 to 773 K. From the XRD patterns, lanthanum hydroxide was transformed into lanthanum oxide at high temperature, and the decrease in hydroxide may result in the decrease in fluoride adsorption capacity. The specific surface area of the samples obtained at 343, 473, and 573 K was 74.9, 68.8, and 64.4 m^2/g, respectively. The Mg–Ce–La adsorbents treated at below 573 K exhibited higher fluoride removal efficiency due to its high specific surface area.

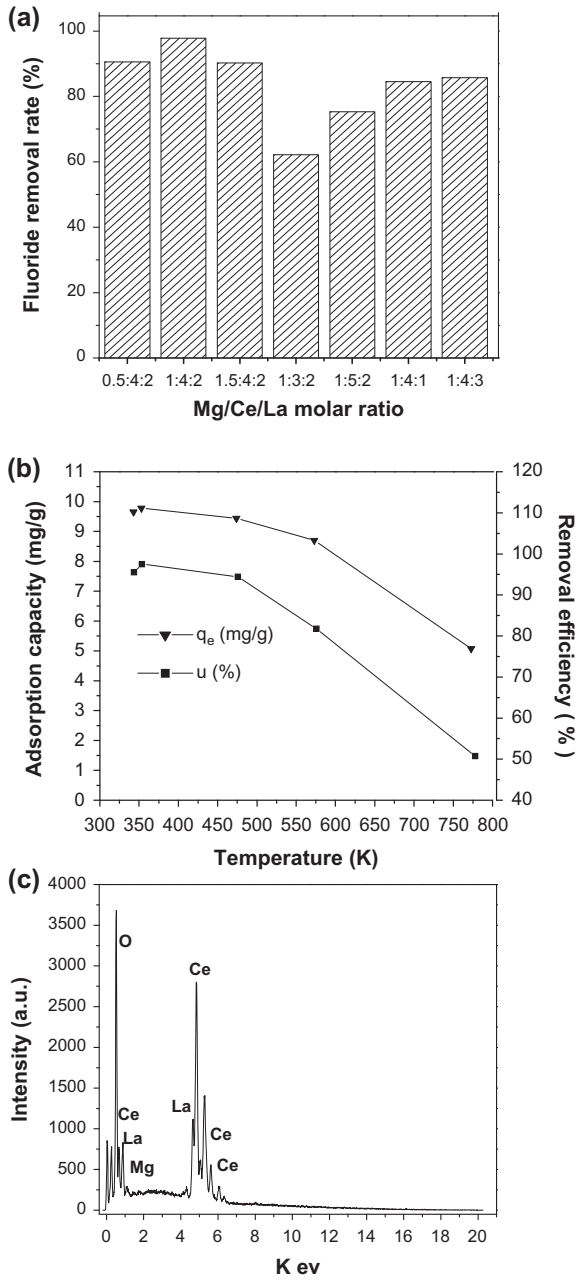

Fig. 1. Fluoride adsorption by the samples prepared at (a) different Mg(II)/La(III)/Ce(III) molar ratios and (b) different temperatures (preparation condition: pH 8.5; adsorption condition: natural pH, shaken at 180 r/min, contact time 40 min, temperature 303 K, adsorbent dose 1.0 g/L); (c) EDX analysis of the Mg–Ce–La adsorbent.

3.2. Characterization

3.2.1. XRD analysis

The XRD patterns of the Mg–Ce–La adsorbent samples treated at different temperatures are showed in Fig. 2(a). The diffraction peaks of $2\theta = 8.6^\circ$ match well with that of $La(NO_3)(OH)_2{\cdot}H_2O$ (JCPD 46-0,346). The peak at $2\theta = 9.1^\circ$ at temperature 353 K corresponds to $La(OH)_2(NO_3)$ (JCPDS 26-1146). A shifting of the peak of $2\theta = 8.6^\circ$ occurred when the

temperature increased from 343 to 353 K which could be ascribed to the evaporation of H_2O with the increase in temperature. In addition, the other diffraction peaks of $2\theta = 28.8^\circ$, 35.5°, 47.4°, and 56.7° are indexed to pure CeO_2 (JCPDS 43-1002) [33]. While the peak at $2\theta = 9.1^\circ$ at 773 K disappeared, implying the decomposition of $La(OH)_2(NO_3)$. No peaks correspond to Mg element can be observed in the pattern, which might be attributed to the low content of Mg in the Mg–Ce–La adsorbent. The EDX analysis (Fig. 1(c)) shows that the presence of Mg, Ce, La, and O on the surface of the Mg–Ce–La adsorbent and the raw adsorbent is composed of MgO, $La(OH)_2(NO_3)$, and CeO_2.

3.2.2. FTIR analysis

The FTIR spectra of the Mg–Ce–La adsorbent before and after fluoride adsorption are depicted in Fig. 2(b). The band at 3,420 cm^{-1} was assigned to the stretching and bending vibration of H_2O in the surface of the adsorbent [34]. The band at 1,680 cm^{-1} was characteristic of hydroxide radical (–OH) stretching vibration and the bands at 490 and 856 cm^{-1} were assigned to metal-oxygen stretching vibration [34,35]. Moreover, the band at 1,380 cm^{-1} was attributed to the asymmetric NO_3^- stretching vibration [36]. NO_3^- may come from the nitrates in the preparation process. The peak intensity at 1,680 cm^{-1} decreased, suggesting

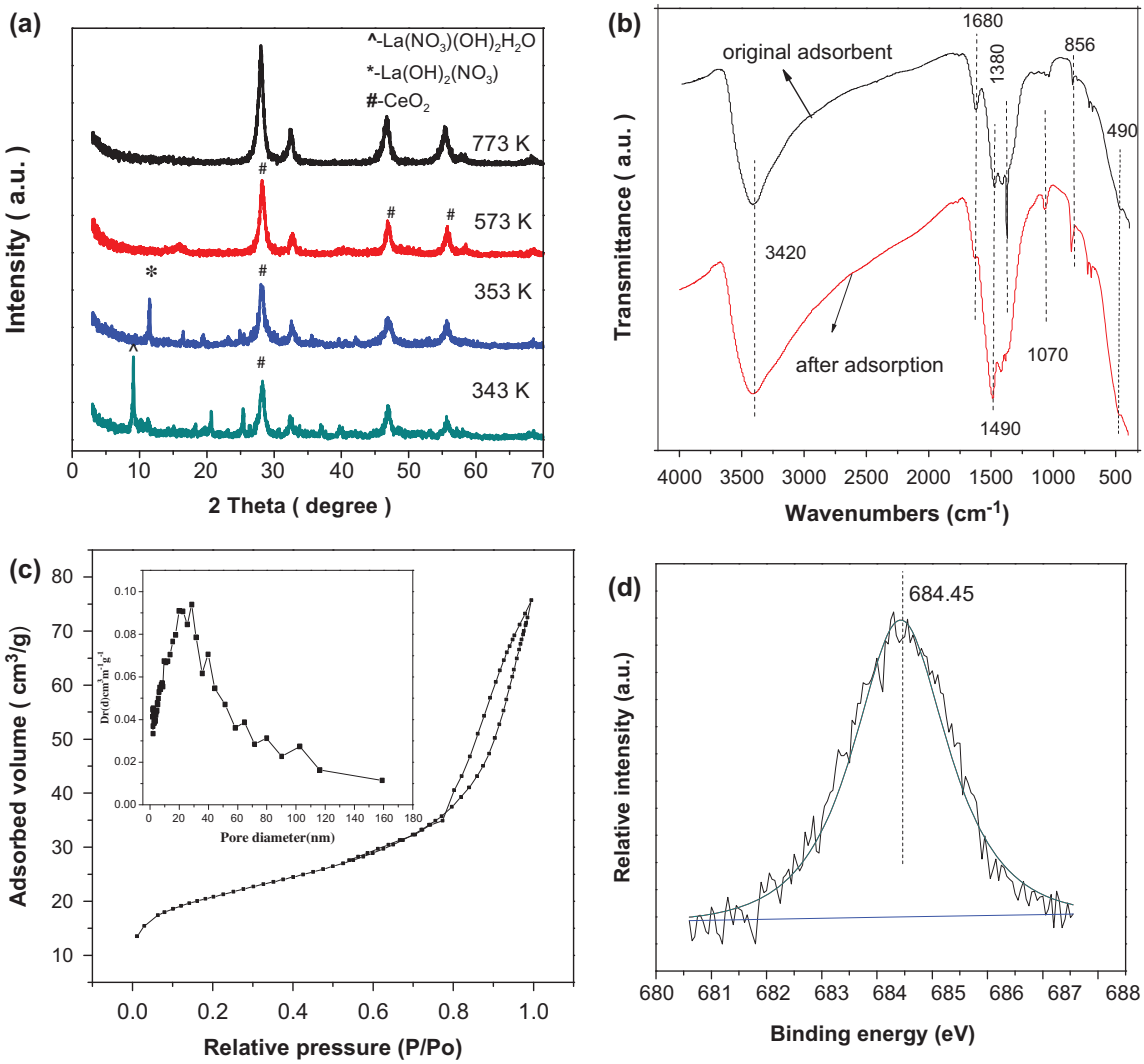

Fig. 2. (a) XRD patterns of the Mg–Ce–La adsorbents at different temperatures, (b) FTIR spectra of the Mg–Ce–La adsorbents before and after adsorption, (c) N_2 adsorption desorption isotherm and pore size distribution of the Mg–Ce–La adsorbent, and (d) High-resolution XPS spectrum of F 1s on the surface of the Mg–Ce–La adsorbent after adsorption.

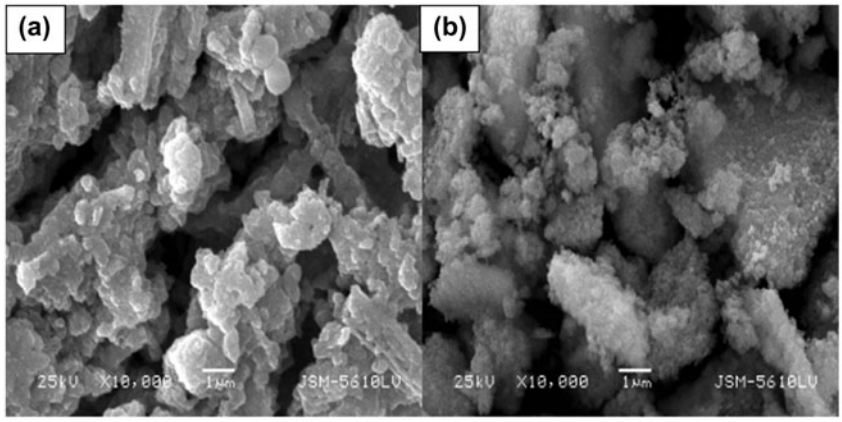

Fig. 3. The SEM images of (a) the raw adsorbent and (b) the adsorbent after adsorption.

that the hydroxide radical (–OH) on the surface of adsorbent was involved in the adsorption reaction [2,37]. It is worth noting that the new bands at 1,070 and 1,490 cm^{-1} appeared, indicating the formation of new chemical bond after fluoride adsorption. The decrease in the peak at 1,680 cm^{-1} may diverge to two separate peaks at 1,490 and 1,070 cm^{-1} after fluoride adsorption [30].

3.2.3. Nitrogen adsorption–desorption analysis

Fig. 2(c) shows the result of N_2 adsorption–desorption analysis. N_2 adsorption–desorption isotherm of the Mg–Ce–La adsorbent is the type IV (IUPAC) with obvious hysteresis hoops of type H3 and exhibits a sharper mesoporous condensation behavior, as reflected in the pore size distribution calculated (Fig. 2(c), inset). The specific surface area of the Mg–Ce–La adsorbent was 118.6 m^2/g calculated by BET model.

3.2.4. XPS and SEM analyses

Fig. 2(d) shows F 1s high-resolution XPS spectrum of the Mg–Ce–La adsorbent after adsorption. A new F 1s peak of the adsorbent after fluoride adsorption is found at binding energy of 684.45 eV, indicating the successfully adsorption of fluoride onto the adsorbent surface [38]. The high fluoride removal rate of the Mg–Ce–La adsorbent can be attributed to the ion-exchange on the adsorbent [39–41].

The SEM images of the raw adsorbent and the adsorbent after adsorption were presented in Fig. 3(a) and (b). The SEM images reveal that the Mg–Ce–La adsorbent has smooth surface and is formed of irregular aggregates. The surface of the Mg–Ce–La adsorbent after adsorption is coarse and shows spongy structure on the surface.

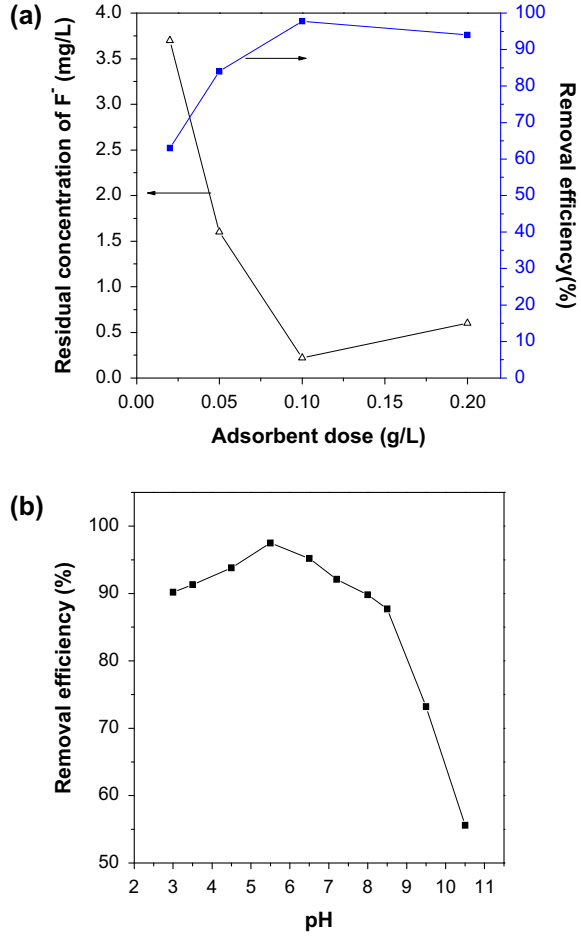

Fig. 4. Effect of (a) adsorbent dose and (b) solution pH on fluoride removal (shaken at 180 r/min, contact time 40 min, adsorbent dose 1.0 g/L).

3.3. Adsorption studies

3.3.1. Effect of adsorbent dosage on fluoride removal

The influence of adsorbent dosage on fluoride removal is depicted in Fig. 4(a). The results reveal that the uptake of fluoride was significantly influenced by the adsorbent dose. The fluoride removal sharply increased from 63.2 to 97.8% after 40 min reaction with an increase in adsorbent dose from 0.2 to 1.0 g/L, which more active sites were available for fluoride removal. However, the fluoride removal efficiency dropped slightly when the adsorbent dose was increased to 2.0 g/L, which could be due to the inhibition effect by excess adsorbent dose. The results are consistent with the theory of heterogeneous surface sites of oxide systems [42].

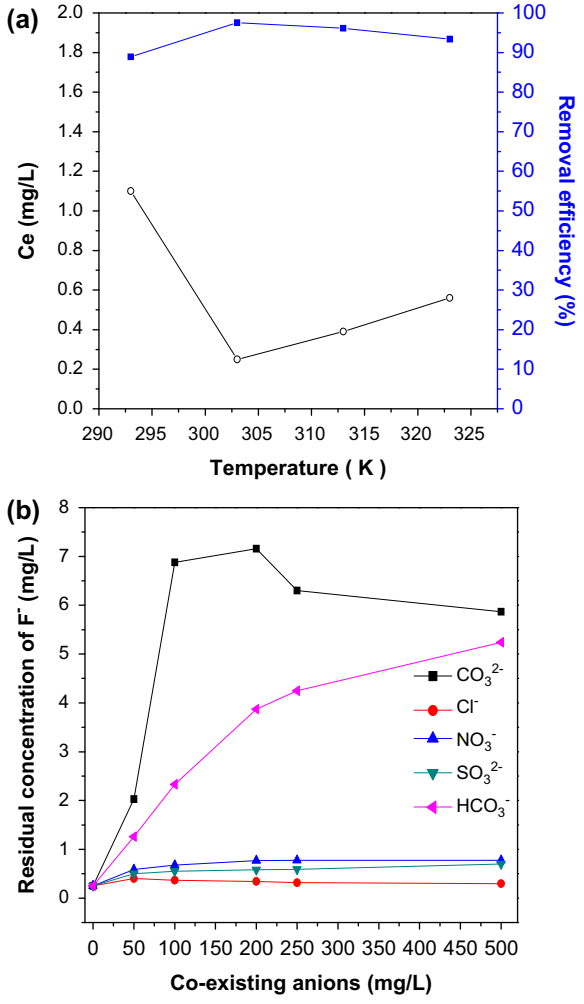

Fig. 5. Effect of (a) solution temperature and (b) coexisting anions on fluoride removal (shaken at 180 r/min, contact time 40 min, adsorbent dose 1.0 g/L).

3.3.2. Effects of solution pH and solution temperature on defluoridation

The effects of initial solution pH on defluoridation are given in Fig. 4(b). Obviously, the fluoride removal rate by the Mg–Ce–La adsorbent increased over the pH range of 3.0–6.0, then decreased significantly with further increasing pH to 10.0. However, the fluoride removal rates could reach above 90% over pH range of 3.0–8.0, which indicates its practical application potential. At higher pH, OH groups would compete with fluoride, which resulted in the decrease in fluoride removal rate.

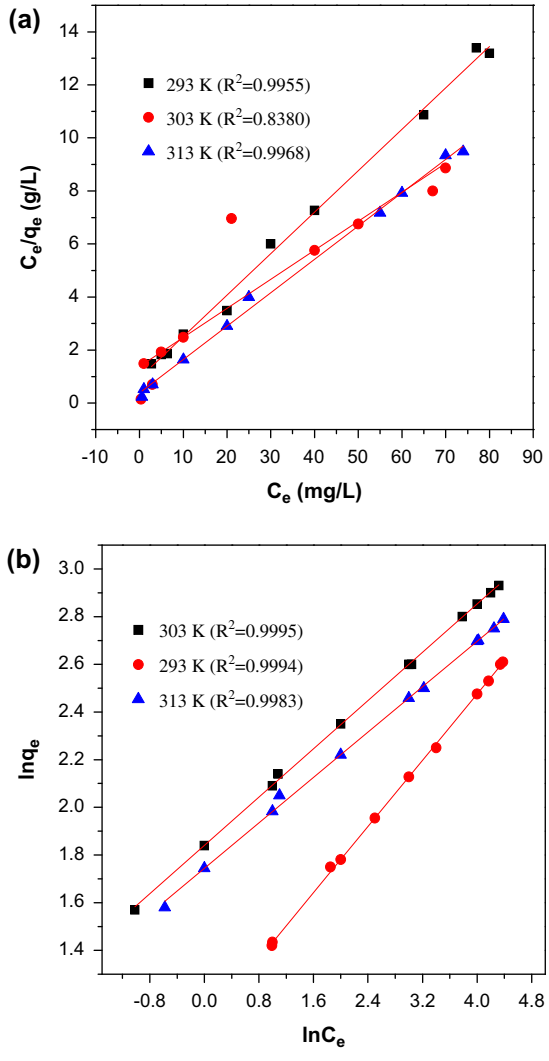

Fig. 6. (a) Langmuir adsorption isotherms and (b) Freundlich adsorption isotherms for the fluoride adsorption on the Mg–Ce–La adsorbent at different temperatures (initial fluoride concentration 10 mg/L, natural pH, shaken at 180 r/min and adsorbent dose 1.0 g/L).

The influence of solution temperatures onto fluoride removal by the Mg–Ce–La adsorbent is showed in Fig. 5(a). The fluoride removal rate was increased with increasing the solution temperature from 293 to 303 K. However, the fluoride removal rate was not obviously affected with further increasing the temperature to 323 K. Defluoridation efficiency of the Mg–Ce–La adsorbent maintained about 90% in the temperatures range from 293 to 323 K.

3.3.3. Effect of coexisting anions on defluoridation

Natural water which was polluted by fluoride contaminant simultaneously contains many types of coexisting anions, such as chlorine ion, nitrate ion, carbonate ion, bicarbonate ion and sulfate ion, and these ions may affect the uptake of fluoride. The effects of different coexisting on fluoride removal by the Mg–Ce–La adsorbent are shown in Fig. 5(b). There is slight influence of fluoride adsorption with increasing chlorine ion concentrations from 0 to 500 mg/L. When the concentrations of NO_3^- and SO_4^{2-} were increased from 0 to 500 mg/L, the defluoridation rates were only reduced by 1 and 5%, respectively. The fluoride removal apparently decreased from 97.5 to 47.5% with increasing the carbonate and bicarbonate concentrations from 0 to 500 mg/L. Therefore, the fluoride removal rate of the Mg–Ce–La adsorbent can significantly be affected by carbonate and bicarbonate ions. The influence extent of different anions is associated with the concentrations and their affinities for the adsorbent. The reduction in fluoride removal in the presence of carbonate and bicarbonate ions may be due to competition from these ions on active sorption site [43]. Therefore, the fluoride adsorption was inhibited in the following order: $CO_3^{2-} > HCO_3^- > SO_4^{2-} > NO_3^- > Cl^-$.

3.3.4. Adsorption isotherm

The experimental data were fitted with the Freundlich model and the Langmuir model. The fluoride adsorption capacity of the Mg–Ce–La adsorbent was calculated using the Freundlich [44] or the Langmuir isotherm [45].

The Freundlich isotherm equation is

$$\ln q_e = \ln K + \frac{1}{n} \ln C_e \tag{3}$$

In Eq. (3), K and n are the Freundlich isotherm constants and n is associated with the temperature. The adsorption capacity increases with the increase of n values, and n lying between 2 and 10 indicates that the environments are favorable for adsorption. The plots of ln q_e versus ln C_e are shown in Fig. 6(a). K and n are calculated from the slope and intercept of plots, respectively.

Table 1
Calculated equilibrium parameters of Langmuir and Freundlich isotherms for fluoride adsorption on the Mg–Ce–La adsorbent

	Langmuir isotherms				Freundlich isotherms		
T (K)	q_{max} (mg/g)	b (L/mg)	R^2	R_L	K ((mg/g)(L/mg)$^{1/n}$)	n	R^2
293	6.446	0.1465	0.9955	0.4057	2.9660	2.8819	0.9994
303	9.140	0.0790	0.8380	0.5587	6.3038	3.9557	0.9995
313	7.957	0.3214	0.9968	0.2373	5.7218	3.5989	0.9983

Table 2
A comparison of adsorption capacity of the Mg–Ce–La adsorbent with other adsorbents in literatures

Adsorbent	Adsorption capacity (mg/g)	Reference
Activated alumina	2.14	[18]
Fe(III)-Zr(IV) hybrid oxide	8.21	[28]
Iron(III)-tin(IV) mixed oxide	10.47	[24]
Fe–Al–Ce adsorbent	2.22	[33]
Ca–Al–La composite	29.30	[39]
Zn-Al layered double hydrosides	4.16	[31]
Mg–Ce–La adsorbent	37.43	In present paper

The Langmuir isotherm equation is

$$\frac{C_e}{q_e} = \frac{1}{Qb} + \frac{C_e}{Q} \tag{4}$$

In Eq. (4), Q and b are the Langmuir isotherm constants, and Q is associated with the temperature. The adsorption capacity increased with increasing the value of Q. The plots of C_e/q_e vs. C_e are shown in Fig. 6(b). Q and b are calculated from the slope and intercept of plots. The parameters of Freundlich isotherm and Langmuir isotherm are summarized in Table 1.

The Fig. 6 illustrates that the Freundlich isotherm (R^2 = 0.9983–0.9995) better describes the experimental data than the Langmuir isotherm (R^2 = 0.8380–0.9968). From the Table 1, n is lying between 2 and 10, suggesting that the adsorbent is effective on defluoridation. In addition, adsorption capacity of the Mg–Ce–La adsorbent was also compared with other adsorbents reported in literatures (Table 2). The Mg–Ce–La adsorbent showed the higher adsorption capacity as compared to other adsorbents, which indicates that the Mg–Ce–La adsorbent could be a potential material for fluoride removal.

3.3.5. Adsorption kinetics

It is greatly important to determine the adsorption kinetics of fluoride onto the adsorbent for its practical application. The results of adsorption kinetics are given in Fig. 7(a). The fluoride adsorption rapidly increased in 20 min, and approximately 80% of fluoride removal rate was reached. In the following period, the fluoride adsorption capacity slowly increased and the adsorption process finally reached the adsorption equilibrium within 40 min.

Pseudo-first-order rate model and pseudo-second-order rate model are applied to analyze the kinetic data. The Eqs. (5) and (6) describe pseudo-first-order rate model and pseudo-second-order rate model [46,47].

$$\ln(q_e - q_t) = \ln q_e - k_1 t \tag{5}$$

$$\frac{t}{q_t} = \frac{1}{k_2 q_e^2} + \frac{t}{q_e} \tag{6}$$

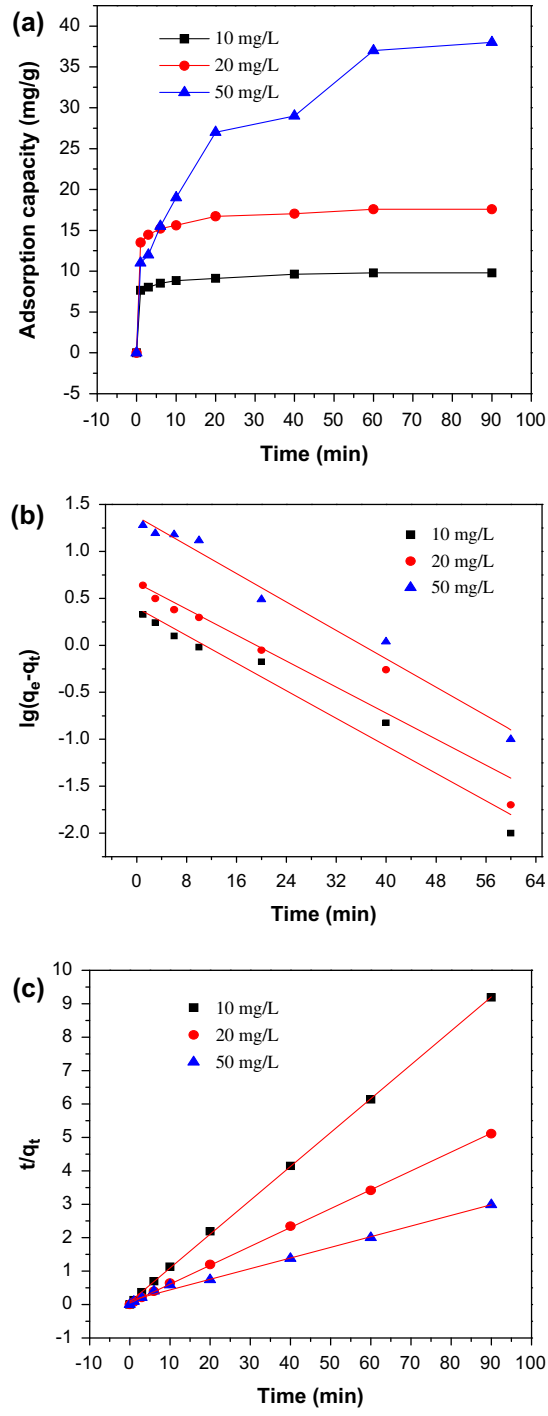

Fig. 7. (a) Kinetic curve of fluoride adsorption on the Mg–Ce–La adsorbent in different fluoride concentrations; (b) Pseudo-first-order kinetic model; and (c) Pseudo-second-order kinetic model for the fluoride adsorption with different fluoride concentrations (natural pH, T = 303 K, adsorbent dose 1.0 g/L).

where q_e and q_t (mg/g) are the adsorption capacity at equilibrium and time t; k_1 (min^{-1}) and k_2 ($g\ mg^{-1}\ min^{-1}$) are the rate constant of pseudo-first-order rate model and pseudo-second-order rate model. The kinetic results are shown in Fig. 7(b) and (c) and Table 3.

As shown in the Fig. 7 and Table 3, the adsorption process is fitted better with the pseudo-second-order rate model (the value of correlation coefficient, $R^2 = 0.9997$) as compared to the pseudo-first-order rate model ($R^2 = 0.9599$). In addition, the experimental adsorption capacity value ($q_{e,exp,}$ 9.78 mg/g) is similar to the calculated adsorption capacity ($q_{e,cal}$, 9.84 mg/g). These results also indicate that fluoride adsorption is well described by the pseudo-second-order model.

3.4. Adsorption thermodynamics

In order to evaluate the thermodynamic behavior of fluoride adsorption onto the Mg–Ce–La adsorbent has been studied. Thermodynamic parameters, such as standard Gibbs free energy change (ΔG), standard enthalpy change (ΔH), and standard entropy change (ΔS) were obtained by the following equations:

$$K_d = \frac{C_{Ae}}{C_{se}} \tag{7}$$

$$\Delta G = -RT \ln K_d \tag{8}$$

$$\Delta G = \Delta H - T\Delta S \tag{9}$$

In Eqs. (7), (8), and (9), K_d is the distribution coefficient (L/g), C_{Ae} is the adsorption amount (mg/g), C_{se} is the equilibrium concentration of fluoride ions, and R is the universal gas constant (J/mol K).

The values of ΔG, ΔH, and ΔS are represented in Table 4. The ΔG was found to be –3.64, –3.89, –3.74, and –3.70 kJ/mol at 293, 303, 313, and 323 K, respectively. The values of ΔG were negative at all temperature (293–323 K), displaying the spontaneous nature of fluoride adsorption by the Mg–Ce–La adsorbent. ΔG value decreased and then increased with increasing the temperature, suggesting less adsorption feasibility at higher temperature and 303 K favors fluoride adsorption. The value of ΔH was positive, further confirming the endothermic nature for fluoride adsorption on the Mg–Ce–La adsorbent. The value of ΔH ranging from 20.9 to 418 kJ/mol showed that the fluoride uptake by the Mg–Ce–La adsorbent occurred via chemisorption.

3.5. Reuse and stability of the adsorbent

The recycled fluoride adsorption experiment was conducted with the original and regenerated adsorbent to detect the reusability and stability of the adsorbent. The results are given in Fig. 8. The fluoride removal rate of original Mg–Ce–La adsorbent was 97.8%, and then defluoridation rate was 94.6, 90.6, 90.0, 88.5, 86.8, and 83.4% with increasing the cycle numbers, respectively. The regenerated adsorbent still showed high fluoride removal rate after four cycles of desorption–adsorption, suggesting the good reusability

Table 3
Calculated kinetics parameters of pseudo-first-order and pseudo-second-order models for fluoride adsorption process on the Mg–Ce–La adsorbent at different fluoride concentrations

C_0 (mg/L)	$q_{e,exp}$ (mg/g)	Pseudo-first-order			Pseudo-second-order		
		$q_{e,cal}$ (mg/g)	k_1 (1/min)	R^2	$q_{e,cal}$ (mg/g)	k_2 (g/(mg min))	R^2
10	9.78	3.43	0.03668	0.9599	9.8328	0.1415	0.9997
20	17.58	4.48	0.03464	0.9047	17.6991	0.0731	0.9989
50	37.00	9.07	0.03784	0.9770	37.4268	0.0085	0.9930

Table 4
Calculated thermodynamic parameters for fluoride adsorption on the Mg–Ce–La adsorbent

Temperature (K)	ΔG (kJ/mol)	ΔH (kJ/mol)	ΔS (J/mol K)
293	−3.64		
303	−3.84	3.89	24.02
313	−3.58		

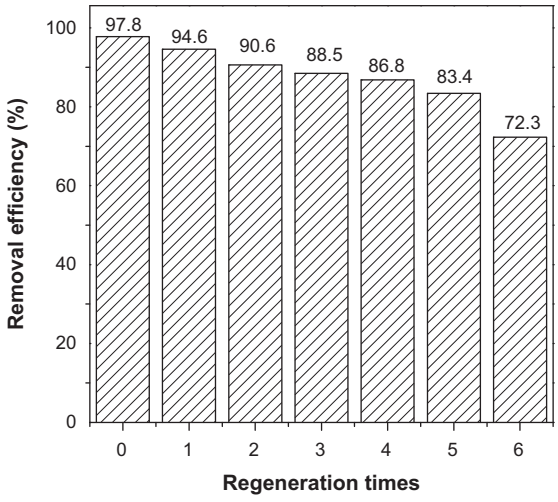

Fig. 8. Reuse test of the adsorbent.

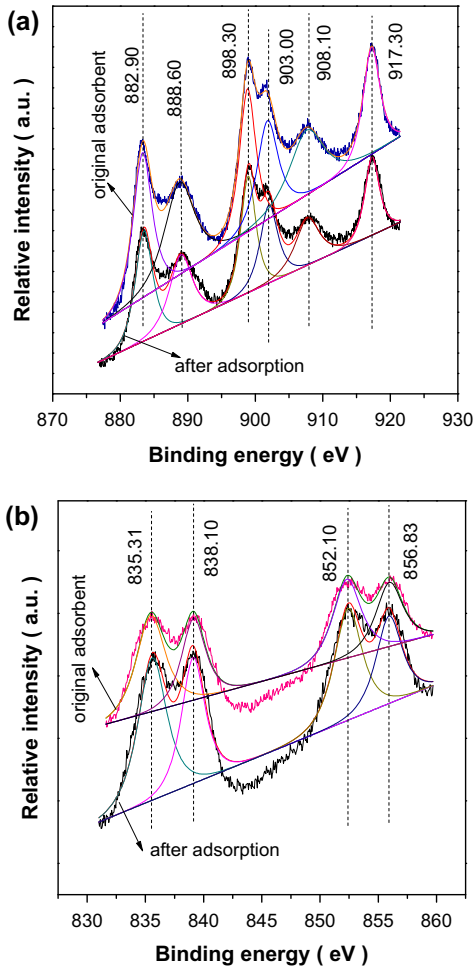

Fig. 9. High-resolution XPS spectra of (a) Ce 3d and (b) La 3d on the surface of the Mg–Ce–La adsorbent before and after adsorption.

and stability of Mg–Ce–La adsorbent. In addition, the adsorbent can be separated easily and recycled by a facile method.

Furthermore, the result of AES analysis showed that there are no metal ions leaching into the solution after adsorption, suggesting the stability of the Mg–Ce–La adsorbent. Therefore, the Mg–Ce–La adsorbent would be stable on the uptake of fluoride. In order to further confirm the stability of the Mg–Ce–La adsorbent, Ce 3d and La 3d high-resolution XPS spectra of the Mg–Ce–La adsorbent before and after adsorption are shown in Fig. 9(a) and (b). As seen in the Fig. 9 (a), the Ce 3d spectra prominently can be divided into six peaks. The binding energy of Ce (III) $3d_{5/2}$ is located at 882.90, 888.60, and 898.30 eV, and the binding energy of Ce (IV) $3d_{3/2}$ is located at 903.00, 908.10, and 917.30 eV [48]. As seen in the Fig. 9(b), the binding energy of La (III) $3d_{3/2}$ is located at 852.10 and 856.83 eV, respectively. The binding energy of La (II) $3d_{5/2}$ is located at 835.31 and 838.10 eV, respectively [49]. The XPS spectra of the Mg–Ce–La adsorbent before and after adsorption show little difference, which confirms that the Mg–Ce–La adsorbent is very stable.

4. Conclusion

An effective and novel Mg–Ce–La adsorbent was prepared by a facile co-precipitation of Mg(II), La(III), and Ce(III) nitrates for fluoride removal. A high fluoride adsorption capacity of 38 mg/g was acquired under an initial fluoride concentration of 50 mg/L, 1.0 g/L adsorbent and 303 K temperature condition. The Mg–Ce–La adsorbent displayed good adsorption property of fluoride over a wide pH range from 3.0 to 8.0 and the optimum pH range was between 5.0 and 6.0. In adsorption studies, the adsorbent reaction reached its equilibrium in about 40 min. The adsorption isotherm could be better described by the Freundlich model than the Langmuir model. Kinetic study results indicate that the fluoride adsorption by the Mg–Ce–La adsorbent followed the pseudo-second-order model. The fluoride adsorption cannot be affected by temperature, sulfate, nitrate, and chloride ions. In addition, the Mg–Ce–La adsorbent still showed high fluoride removal efficiency after being reused for four cycles, indicating that the adsorbent is a promising material for fluoride removal from water.

Acknowledgments

This work was supported by National Key Technology R&D Program of China (2012BAJ25B02-03).

References

[1] B. Zhao, Y. Zhang, X.M. Dou, X.M. Wu, M. Yang, Granulation of Fe–Al–Ce trimetal hydroxide as a fluoride adsorbent using the extrusion method, Chem. Eng. J. 185–186 (2012) 211–218.

[2] A. Bhatnagar, E. Kumar, M. Sillanpää, Fluoride removal from water by adsorption, Chem. Eng. J. 171 (2011) 811–840.

[3] M.S. Masoud, G.F. El-Said, Behavior of some chloride, carbonate, phosphate, sulphate and borate additive salt-NaCl aqueous solution systems in the absence and presence of NaF, Desalin. Water Treat. 29 (2011) 1–9.

[4] S. Ayoob, A.K. Gupta, Fluoride in drinking water: A review on the status and stress effects, Crit. Rev. Environ. Sci. Technol. 36 (2006) 433–487.

[5] J.J. Shen, A. Schäfer, Removal of fluoride and uranium by nanofiltration and reverse osmosis: A review, Chemosphere 117 (2014) 679–691.

[6] R. Malaisamy, A. Talla-Nwafo, K.L. Jones, Polyelectrolyte modification of nanofiltration membrane for selective removal of monovalent anions, Sep. Purif. Technol. 77 (2011) 367–374.

[7] E. Erdem, T. Ali, C. Yunus, K. Izzet, Electrodialytic removal of fluoride from water: Effects of process parameters and accompanying anions, Sep. Purif. Technol. 64 (2008) 147–153.

[8] P.K. Holt, G.W. Barton, C.A. Mitchell, The future for electrocoagulation as a localised water treatment technology, Chemosphere 59 (2005) 355–367.

[9] O.T. Can, M. Kobya, E. Demirbas, M. Bayramoglu, Treatment of the textile wastewater by combined electrocoagulation, Chemosphere 62 (2006) 181–187.

[10] E. Kir, E. Alkan, Fluoride removal by Donnan dialysis with plasma-modified and unmodified anion-exchange membranes, Desalination 197 (2006) 217–224.

[11] A. Tor, Removal of fluoride from water using anion-exchange membrane under Donnan dialysis condition, J. Hazard. Mater. 141 (2007) 814–818.

[12] S. Aoudj, A. Khelifa, N. Drouiche, M. Hecini, Development of an integrated electro-coagulation–flotation for semiconductor wastewater treatment, Desalin. Water Treat. 55 (2015) 1422–1432.

[13] A. Yuchi, K. Matsunaga, T. Niwa, H. Terao, H. Wada, Separation and preconcentration of fluoride at the ng ml^{-1} level with a polymer complex of zirconium (IV) followed by potentiometric determination in a flow system, Anal. Chim. Acta 388 (1999) 201–208.

[14] Meenakshi, R.C. Maheshwari, Fluoride in drinking water and its removal, J. Hazard. Mater. 137 (2006) 456–463.

[15] J.X. Kang, B. Li, J. Song, D. Li, J. Yang, W. Zhan, D.Q. Liu, Defluoridation of water using calcined magnesia/pullulan composite, Chem. Eng. J. 166 (2011) 765–771.

[16] D.D. Tang, Y.W. Zhao, Y.X. Wang, Y.J. Yang, D.Y. Li, T.W. Peng, X.H. Mao, Defluorination from aqueous solution by Ti(IV)-modified granular activated carbon, Desalin. Water Treat. 54 (2015) 3432–3443.

[17] W. Wei, X. Wang, Y. Wang, M. Xu, J. Cui, Z.G. Wei, Evaluation of removal efficiency of fluoride from aqueous solution using nanosized fluorapatite, Desalin. Water Treat. 52 (2014) 6219–6229.

[18] S. Ghorai, K.K. Pant, Equilibrium, kinetics and breakthrough studies for adsorption of fluoride on activated alumina, Sep. Purif. Technol. 42 (2005) 265–271.

[19] W.X. Gong, J.H. Qu, R.P. Liu, H.C. Lan, Adsorption of fluoride onto different types of aluminas, Chem. Eng. J. 189–190 (2012) 126–133.

[20] S. Mandal, S. Mayadevi, Defluoridation of water using as-synthesized Zn/Al/Cl anionic clay adsorbent: Equilibrium and regeneration studies, J. Hazard. Mater. 167 (2009) 873–878.

[21] M.G. Sujana, H.K. Pradhan, S. Anand, Studies on sorption of some geomaterials for fluoride removal from aqueous solutions, J. Hazard. Mater. 161 (2009) 120–125.

[22] M. Islam, R.K. Patel, Evaluation of removal efficiency of fluoride from aqueous solution using quick lime, J. Hazard. Mater. 143 (2007) 303–310.

[23] J.Y. Du, D.A. Sabatini, E.C. Butler, Synthesis, characterization, and evaluation of simple aluminum-based adsorbents for fluoride removal from drinking water, Chemosphere 101 (2014) 21–27.

[24] K. Biswas, K. Gupta, U.C. Ghosh, Adsorption of fluoride by hydrous iron(III)–tin(IV) bimetal mixed oxide from the aqueous solutions, Chem. Eng. J. 149 (2009) 196–206.

[25] L. Chen, H.X. Wu, T.J. Wang, Y. Jin, Y. Zhang, X.M. Dou, Granulation of Fe-Al-Ce nano-adsorbent for fluoride removal from drinking water by spray coating on sand in a fluidized bed, Powder Technol. 193 (2009) 59–64.

[26] A.M. Raichur, M.J. Basu, Adsorption of fluoride onto mixed rare earth oxides, Sep. Purif. Technol. 24 (2001) 121–127.

[27] S.M. Prabhu, S. Meenakshi, Defluoridation of water using synthesized Zr(IV) encapsulated silica gel/chitosan biocomposite: Adsorption isotherms and kinetic studies, Desalin. Water Treat. 53 (2015) 3592–3603.

[28] K. Biswas, D. Bandhoyapadhyay, U.C. Ghosh, Adsorption kinetics of fluoride on iron(III)-zirconium (IV) hybrid oxide, Adsorption 13 (2007) 83–94.

[29] Y. Zhang, M. Yang, X. Huang, Arsenic(V) removal with a Ce(IV) doped iron oxide adsorbent, Chemosphere 51 (2003) 945–952.

[30] Y. Zhang, M. Yang, X.M. Dou, H. He, D.S. Wang, Arsenate adsorption on an Fe−Ce bimetal oxide adsorbent: Role of surface properties, Environ. Sci. Technol. 39 (2005) 7246–7253.

[31] S. Mandal, S. Mayadevi, Adsorption of fluoride ions by Zn-Al layered double hydroxides, Appl. Clay Sci. 40 (2008) 54–62.

[32] S. Moriyama, K. Sasaki, T. Hirajima, Effect of calcination temperature on Mg-Al bimetallic oxides as sorbents for the removal of F in aqueous solutions, Chemosphere 95 (2004) 597–603.

[33] X.Y. Wang, L. Ran, Y. Dai, Y.J. Lu, Q.G. Dai, Removal of Cl adsorbed on Mn-Ce-La solid solution catalysts during CVOC combustion, J. Colloid Interface Sci. 426 (2014) 324–332.

[34] J.M. Pan, X.H. Zou, X. Wang, W. Guan, Y.S. Yan, J. Han, Selective recognition of 2, 4-dichlorophenol from aqueous solution by uniformly sized molecularly imprinted microspheres with β-cyclodextrin/attapulgite composites as support, Chem. Eng. J. 162 (2010) 910–918.

[35] Z.J. Li, S.B. Deng, G. Yu, J. Huang, V. Lim, As(V) and As(III) removal from water by a Ce-Ti oxide adsorbent: Behavior and mechanism, Chem. Eng. J. 161 (2010) 106–113.
[36] F. Long, J.L. Gong, G.M. Zeng, L. Chen, X.Y. Wang, J.H. Deng, Q.Y. Niu, H.Y. Zhang, X.R. Zhang, Removal of phosphate from aqueous solution by magnetic Fe-Zr binary oxide, Chem. Eng. J. 171 (2011) 448–455.
[37] R.L. Frost, Y.F. Xi and H.P. He, Synthesis, characterization of palygorskite supported zero-valent iron and its application for methylene blue adsorption, J. Colloid Interface Sci. 341 (2010) 153–161.
[38] W. Xiang, G.K. Zhang, Y.L. Zhang, D.D. Tang, J.T. Wang, Synthesis and characterization of cotton-like Ca-Al-La composite as an adsorbent for fluoride removal, Chem. Eng. J. 250 (2014) 423–430.
[39] S.M. Maliyekkal, K.R. Antony, T. Pradeep, High yield combustion synthesis of nanomagnesia and its application for fluoride removal, Sci. Total Environ. 408 (2010) 2273–2282.
[40] S.G. Wang, Y. Ma, Y.J. Shi, W.X. Gong, Defluoridation performance and mechanism of nano-scale aluminum oxide hydroxide in aqueous solution, J. Chem. Technol. Biotechnol. 84 (2009) 1043–1050.
[41] D.D. Tang, G.K. Zhang, Efficient removal of fluoride by hierarchical Ce-Fe bimetal oxides adsorbent: Thermodynamics, kinetics and mechanism, Chem. Eng. J. 283 (2016) 721–729.
[42] Z.Q. He, X. Xu, S. Song, L. Xie, J.J. Tu, J.M. Chen, B. Yan, A Visible light-driven titanium dioxide photocatalyst codoped with lanthanum and iodine: An application in the degradation of oxalic acid, J. Phys. Chem. C 112 (2008) 16431–16437.
[43] G.K. Zhang, Z.L. He, W. Xu, A low-cost and high efficient zirconium-modified-Na-attapulgite adsorbent for fluoride removal from aqueous solutions, Chem. Eng. J. 183 (2012) 315–324.
[44] H. Freundlich, Über die adsorption in lösungen, Z. Phys. Chem. 57 (1906) 385–470.
[45] I. Langmuir, The constitution and fundamental properties of solids and liquids. Part I. Solids, J. Am. Chem. Soc. 38 (1916) 2221–2295.
[46] Y.S. Ho, G. McKay, Sorption of dye from aqueous solution by peat, Chem. Eng. J. 70 (1998) 115–124.
[47] G. Blanchard, M. Maunaye, G. Martin, Removal of heavy metals from waters by means of natural zeolites, Water Res. 18 (1984) 1501–1507.
[48] T.W. Hamann, A.B.F. Martinson, J.W. Elam, M.J. Pellin, J.T. Hupp, Atomic layer deposition of TiO 2 on aerogel templates: New photoanodes for dye-sensitized solar cells, J. Phys. Chem. C 112 (2008) 10303–10307.
[49] M. Srivastava, A.K. Das, P. Khanra, M.E. Uddin, N.H. Kim, J.H. Lee, Characterizations of in situ grown ceria nanoparticles on reduced graphene oxide as a catalyst for the electrooxidation of hydrazine, J. Mater. Chem. A 1 (2013) 9792–9801.